



Bone marrow edema around the hip in non-traumatic pain: dual-energy CT vs MRI

Giovanni Foti¹ · Niccolò Faccioli² · Ronaldo Silva³ · Eugenio Oliboni¹ · Claudio Zorzi⁴ · Giovanni Carbone¹

Received: 15 January 2020 / Revised: 14 February 2020 / Accepted: 21 February 2020 / Published online: 12 March 2020
© European Society of Radiology 2020

Abstract

Objectives To evaluate the diagnostic accuracy of dual-energy computed tomography (DECT) in identifying bone marrow edema (BME) around the hip joint in non-traumatic patients.

Methods This prospective IRB-approved study was conducted between January 2019 and October 2019 and included 59 consecutive patients (18 males, 41 females; mean age 61.5 years, range 32–82) who were assessed by DECT and magnetic resonance imaging (MRI) within a 5-day period. Diagnostic accuracy values for diagnosing BME on a per-patient and on a per-partition-basis analysis were calculated for DECT images by two readers (R1 and R2, with 15 and 10 years of experience, respectively), using MRI as reference for diagnosis. Inter-observer agreements were calculated with k -statistics. A p value of <0.05 was considered as statistically significant.

Results MRI depicted BME in 44/59 patients (74.58%), with the involvement of 83/708 (11.72%) partitions. The sensitivity, specificity, and accuracy of R1 and R2 were 95.45% (42/44), 86.67% (13/15), and 93.22% (55/59) for R1, and 86.36% (38/44), 80.00% (12/15), and 84.75% (50/59) for R2. For both readers, the BME detection rate was higher in patients with severe edema (100%) in comparison to patients with mild edema (91.30% and 73.91%). In the partition-basis analysis, sensitivity, specificity, and accuracy ranges were 33.3 to 100%, 91.84 to 100%, and 88.14 to 100%, respectively. The inter-observer agreement for patients' analysis was substantial ($k = 0.7065$), whereas for partition analysis ranged from fair ($k = 0.2976$) to near-perfect ($k = 1.000$).

Conclusion DECT can accurately identify BME around the hip joint, in comparison to MRI.

Key Points

- DECT can accurately identify bone marrow edema around the hip joint in a cohort of non-traumatic patients.
- The detection of bone marrow edema by means of DECT may help the radiologist to identify associated findings, including avascular necrosis of the femoral head and insufficiency or stress fractures.
- In cases of patients suffering from groin pain with bone marrow edema identified by DECT, the concurrent reading of high-resolution conventional CT images may increase the confidence of diagnosis and/or reduce the reading time.

Keywords Hip joint · Magnetic resonance imaging · Multidetector computed tomography · Bone marrow

Abbreviations

AVN Avascular necrosis
BME Bone marrow edema

DECT Dual-energy computed tomography
IRB Institutional Review Board
 k Cohen's kappa coefficient
MRI Magnetic resonance imaging
NPV Negative predictive value
OCL Osteochondral lesions
PPV Positive predictive value
VNCA Virtual non-calcium

✉ Giovanni Foti
gfoti81@yahoo.it; Giovanni.foti@sacrocuore.it

- ¹ Department of Radiology, IRCCS Sacro Cuore Don Calabria Hospital, Via Don A. Sempreboni 10, 37024 Negrar, Italy
- ² Department of Radiology, Verona University Hospital, Verona, Italy
- ³ Clinical Research Unit, IRCCS Sacro Cuore Don Calabria Hospital, Negrar, Italy
- ⁴ Department of Orthopedic Surgery, IRCCS Sacro Cuore Don Calabria Hospital, Negrar, Italy

Introduction

Bone marrow edema (BME) represents an important cause of hip pain [1]. The pathophysiological implications of BME

include a link to bone marrow capillary wall damage, which can lead to increased intraosseous pressure and irritation of the sensory nerves [2]. BME can be diagnosed in patients with either traumatic or non-traumatic hip fractures, and is evident as cases of transient BME of the hip that manifest in advanced osteoarthritis, avascular necrosis (AVN), transient osteoporosis, stress injuries, and infectious or inflammatory diseases [1–5]. Magnetic resonance imaging (MRI) plays a key role in the identification of BME around the hip joint [1]. BME is often highly relevant in the management of pathologies that affect the hip joint [1] as BME can sometimes be the only imaging finding in the early stages of AVN. The treatment of AVN strictly depends on the disease stage, and the success of treatment often depends on the accuracy of stage classification [6–10]. Accurate detection of hip BME is therefore vital in selecting an appropriate disease management strategy. MRI may also reveal subchondral fractures and increased synovial fluid accumulation [11–17]. Furthermore, MRI can differentiate AVN from other entities, including insufficiency fractures [18]. However, MRI cannot be routinely used for all patients owing to its limited availability, contraindications, and/or the presence of metal artifacts. In cases of AVN, computed tomography (CT) may reveal more subchondral fractures of the femoral head than radiography or MRI can [18]. In addition, CT can identify the cortical irregularities and erosions that often characterize infectious or inflammatory diseases [19]. However, conventional CT is unable to identify BME and as such, in the absence of sclerosis, subchondral fracture, or articular irregularities, AVN can be missed [20].

Conversely, dual-energy computed tomography (DECT) has successfully revealed BME in cases of non-displaced fractures [21, 22]. In light of this, the possible role for DECT in the evaluation of non-traumatic patients, including those suffering from AVN of the hip, has recently been proposed [23]. Furthermore, in a recently published paper, dual-energy with water–hydroxyapatite (HAP) imaging showed good diagnostic performance for bone marrow edema in patients with non-traumatic hip pain [24]. Moreover, DECT applications can help reducing metal artifacts around the hip joint, especially when used in combination with additional dedicated CT post-processing algorithms [25]. DECT with virtual non-calcium (VNCa) application has also successfully identified talar dome osteochondral lesions (OCL) in a subgroup of non-traumatic patients [26]. In a clinical setting of worsening groin or hip pain, VNCa techniques could be used to identify BME, which can be key in the diagnosis of multiple diseases. When bone marrow edema is identified on DECT, the confident diagnosis of AVN or subchondral fracture can be achieved with concurrent reading of the virtual non-calcium images and the conventional CT [23].

Further to this, DECT could be an important alternative approach for patients unable to undergo MRI.

The purpose of our study was therefore to investigate the diagnostic accuracy values of DECT in detecting BME in the hip of non-traumatic patients suffering from hip pain, by using MRI as a reference standard.

Materials and methods

Patient population

This prospective study was approved by the Institutional Review Board (IRB). Informed consent was obtained from all enrolled patients. Between January 2019 and October 2019, 69 consecutive patients were considered for inclusion in the study with 59 meeting the inclusion criteria. All patients were referred to our department following an orthopedic visit. Eligibility criteria were represented by acute or worsening pain around the hip joint, in patients with no recent trauma who were assessed by both MRI and DECT within a 5-day period (mean 2 days, range 0–5 days). Exclusion criteria were represented by lack of comparative DECT or MRI scan, and presence of metal hardware around the hip. CT examinations were performed to visualize hip anatomy and to detect any calcifications, subtle fractures, cortical irregularity, or erosive changes. Conversely, MRI examinations were undertaken to assess the presence of BME around the hip.

DECT protocol

The DECT examinations were performed with a third-generation 384-slice dual-source CT scanner (Somatom® Definition Force, Siemens Healthineers). The scanning parameters were as follows: tube A 80 kV and tube B 150 kV with a tin filter. The predefined tube current–time product was set at a ratio of 1.6:1 (tube A, 220 quality reference mAs; tube B, 138 quality reference mAs). Automated attenuation-based tube current modulation (CARE dose 4D; Siemens Healthcare) was used.

The mean effective post-scan volume CT dose index volume (CTDI_{vol}) was 9.37 mGy ± 1.5 (range, 6.8–12.3 mGy); the mean DLP (mGy/cm) was 280.41 (range, 242.22–382.30). Dose parameters are comparable to our current standard CT protocol for the hip.

DECT post-processing

After each DECT scan, three data sets of reconstructed images (thickness, 0.75 mm; increment, 0.60 mm) were made available: an 80-kVp set, a 150-kVp set with a tin filter, and an average-weighted set calculated from both tube data at a ratio of 0.5:0.5 to imitate a single 120-kVp image. Blended virtual 120-kV images (Br 64 Kernel – osteo-window filter) were used for clinical reading. Soft tissue kernel (Qr32) 80-kVp

and 150-kVp set images were transferred to an offline workstation (SyngoVia® VB20; Siemens Healthineers). The DE-specific information was fused with the conventional grayscale morphologic images (thickness, 1 mm; increment, 1 mm).

MRI protocol

MRI was performed with a commercially available 1.5-T unit (Magnetom Avanto Fit; Siemens Healthineers). Standard 4-mm thick T1-weighted turbo spin-echo (TR/TE/FA = 650.0 ms/18.0 ms/150°), T2-weighted turbo spin-echo (TR/TE = 4300.0 ms/124.0 ms), and proton density fat-saturated sequences (TR/TE/FA = 2320.0 ms/39.0 ms/150°) were performed on axial and coronal planes.

Image analysis

All available image data sets for each hip were evaluated for the presence of BME using a binary classification system (1, presence of BME; 0, absence of BME). Each hip was divided into six partitions per side for better analyzing the presence of BME, as follows: partition 1, right femoral neck; partition 2, right femoral head; partition 3, right acetabular roof; partition 4, right pubis; partition 5, right iliac bone; partition 6, right sacral bone; partition 7, left femoral neck; partition 8, left femoral head; partition 9, left acetabular roof; partition 10, left pubis; partition 11, left iliac bone; partition 12, left sacral bone. Therefore, a total of 708 partitions were evaluated in the 59 patients enrolled in the study.

As the reference standard, all MRI images were evaluated in consensus, by two experienced radiologists (with 16 and 22 years of experience), who were blind to clinical and CT findings. For MRI findings, a diagnosis of BME was based on any signal intensity increase on fat sat imaging with signal decay at T1-weighted imaging. Moreover, BME was graded as mild or severe depending on a visual assessment. Associated imaging diagnoses, including AVN, stress, or insufficiency fractures, were also noted.

Standard axial, coronal, and sagittal reconstructed CT and DECT images (2D and 3D color-coded maps) were analyzed by two independent radiologists (with 11 and 15 years of experience) in a random order, blinded to clinical and MRI findings, on a dedicated SyngoVia® workstation. As concerns the default settings for color-coded maps, the range of densities included were set between – 150 HU and 100 HU (Fig. 2a), with superimposed color-coded maps visualized only when density values were above – 50-HU cut-off.

Standard CT findings, including bone sclerosis, subchondral fracture, articular irregularities, or erosions, were evaluated and used for diagnosis. Associated diagnoses, including AVN, stress, or insufficiency fractures, were assessed by DECT. In cases of disagreement on the presence of BME, a

consensus reading was appended, and the consensual results were used for further analysis.

Statistical analysis

With regard to the patient-basis analysis, each reader performed a qualitative assessment for distinguishing presence versus absence of BME. Conversely, the partition-basis analysis was performed after the consensus reading. The sensitivity, specificity, positive predictive values (PPV), negative predictive values (NPV), and accuracy (Acc) of each data set for the diagnosis of BME were calculated on a per-patient and on a per-partition basis. MRI images served as the standard of reference. Inter-observer agreement and intra-observer agreement were calculated by using Cohen's kappa coefficient (*k*). The statistical significance level was fixed at 5%. Data analyses were performed using SAS software version 9.4.

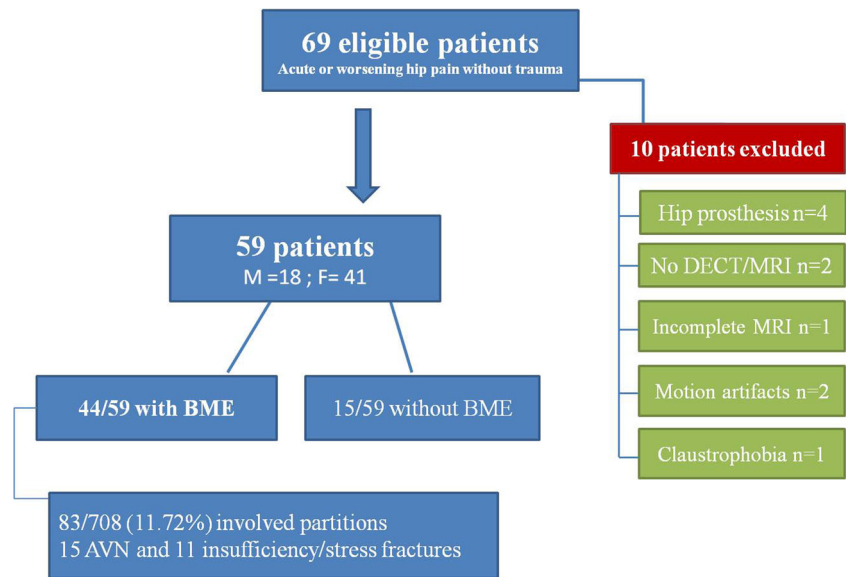
Results

A total of 59 patients were included in this study (mean age 61.5 years, SD 10.3, range 32–82), 18 males (mean age 60.6 years, SD 5.1, range 39–80) and 41 females (mean age 61.9 years, SD 12.2, range 32–82). Ten patients were excluded from the study (mean age 63.5, SD 8.8, range 49–76) for the following reasons: a lack of comparative DECT or MRI scan (*n* = 2), presence of hip prosthesis (*n* = 4), incomplete MRI protocol (*n* = 1), motion artifacts during MRI scanning (*n* = 2), and claustrophobia (*n* = 1). A diagram showing included and excluded patients is shown in Fig. 1. The clinical data of patients enrolled in the study are summarized in Table 1. The diagnostic accuracy values of DECT on a per-patient and on a per-partition-basis analysis are summarized in Tables 2 and 3, respectively.

Patient-basis analysis

BME was depicted by MRI in 44/59 patients (74.58%) and ruled out in 15/59 patients (25.42%). BME as detected by MRI (Figs. 2 and 3) was graded as mild in 23/59 cases (38.98%) and as severe in 21/59 cases (35.59%). Reader 1 (R1) correctly identified the presence of BME in 42/44 patients (95.45% sensitivity). R1 correctly identified the absence of BME in 13/15 patients (86.67% specificity), meaning that two false positive (FP) cases were reported (Fig. 4). The BME detection rate of R1 was 91.30% (21/23 patients) and 100% (21/21 patients) among the subgroups of patients suffering from mild or severe edema, as determined by MRI, respectively. Reader 2 (R2) correctly identified the presence of BME in 38/44 patients (86.36% sensitivity). R2 correctly ruled out the presence of BME in 12/15

Fig. 1 Flowchart of patients included in the study and exclusion criteria



patients (80.00% specificity). The BME detection rate of R2 was 73.91% (17/23 patients) and 100% (21/21

patients) among the subgroups of patients suffering from mild or severe edema, as determined by MRI, respectively.

Table 1 Clinical data of patients enrolled

Parameter	Value
Age* (years)	61.5 (SD = 10.3; 32–82)
Age of male* (years) = n, 18	60.6 (SD = 5.1; 39–80)
Age of female* (years) = n, 41	61.9 (SD = 12.2; 32–82)
Age of excluded* (years) = n, 10	63.5 (SD = 8.8; 49–73)
Interval MRI-DECT	Mean 2 days; range 0–5 days
BME-positive patients	44/59 (74.58%)
BME severe	21/59 (35.59%)
BME mild	23/59 (38.98%)
Total involved partitions	83/708 (11.72%)
Partition 1 (right femoral neck)	12/59 patients (20.34%)
Partition 2 (right femoral head)	17/59 patients (28.81%)
Partition 3 (right acetabular roof)	10/59 patients (16.95%)
Partition 4 (right pubis)	4/59 patients (6.78%)
Partition 5 (right iliac bone)	3/59 patients (5.08%)
Partition 6 (right sacral bone)	4/59 patients (6.78%)
Partition 7 (left femoral neck)	7/59 patients (11.86%)
Partition 8 (left femoral head)	12/59 patients (20.34%)
Partition 9 (left acetabular roof)	6/59 patients (10.57%)
Partition 10 (left pubis)	3/59 patients (5.08%)
Partition 11 (left iliac bone)	3/59 patients (5.08%)
Partition 12 (left sacral bone)	6/59 patients (10.17%)
Patients with additional findings	24/59 (40.67%)
AVN	n = 13 (2 bilateral AVN)
Insufficiency/stress fractures	n = 11

Data are numbers of patients/cases with percentages in parentheses. *Data are expressed as mean and standard deviation (SD) and ranges. BME, bone marrow edema; AVN, avascular necrosis of the femoral head

Partition-basis analysis

The presence of BME was depicted at MRI in 83/708 (11.72%) partitions (range 1 to 8 partitions distributed as 25.42% no partition involved, 38.98% 1 partition involved, 18.64% 2 partitions involved, 13.56% 3 partitions involved, 1.69% 6 partitions involved, and 1.69% 8 partitions involved).

The sensitivity of DECT ranged from 100 to 80.00% for 8/12 partitions and specificity from 100 to 91.84% (Table 3).

Table 2 Diagnostic accuracy parameters of DECT (qualitative assessment performed by reader 1 and reader 2) on a per-patient-based analysis

	Reader 1	Reader 2
TP	42	38
FN	2	6
Sensitivity [95% CI]	95.45 [84.53, 99.44]	83.36 [72.65, 94.83]
TN	13	12
FP	2	3
Specificity [95% CI]	86.67 [59.54, 98.34]	80.00 [(51.91, 95.67]
PPV [95% CI]	95.45 [84.53, 99.44]	92.68 [80.08, 98.46]
NPV [95% CI]	86.67 [59.54, 98.34]	66.67 [40.99, 86.66]
Accuracy [95% CI]	93.22 [83.54, 98.12]	84.75 [73.01, 92.78]

TP, true positive; FN, false negative; TN, true negative; FP, false positive; PPV, positive predictive value; NPV, negative predictive value

Table 3 Diagnostic performance of DECT images (consensus reading performed by reader 1 and reader 2) on a per-partition-based analysis. Data are ordered by sensitivity

P	TP	FN	TN	FP	Sensitivity [95% CI]	Specificity [95% CI]	PPV [95% CI]	NPV [%]	Acc [%]	Agr.
P9	6	0	53	0	100.00 [54.07, 100.00]	100.00 [93.28, 100.00]	100.00 [54.07, 100.00]	100.00 [93.28, 100.00]	100.00 [93.94, 100.00]	1.000
P11	3	0	56	0	100.00 [29.24, 100.00]	100.00 [93.51, 100.00]	100.00 [29.24, 100.00]	100.00 [93.62, 100.00]	100.00 [93.94, 100.00]	1.000
P5	3	0	53	3	100.00 [29.24, 100.00]	94.64 [85.13, 98.88]	50.00 [11.81, 88.19]	100.00 [93.28, 100.00]	94.92 [85.85, 98.94]	.6424 [.2743, 1.0000]
P7	7	0	51	1	100.00 [59.04, 100.00]	98.08 [89.74, 99.95]	0.8750 [47.35, 52.65]	100.00 [93.02, 100.00]	98.31 [90.91, 99.96]	.9237 [.7758, 1.0000]
P8	10	2	46	1	83.33 [51.59, 97.91]	97.87 [88.71, 99.95]	90.91 [58.72, 99.77]	95.83 [85.75, 99.49]	94.92 [85.85, 98.94]	.8381 [.6606, 1.0000]
P12	5	1	49	4	83.33 [35.88, 99.58]	92.45 [81.79, 97.91]	55.56 [21.20, 86.30]	98.00 [89.35, 99.95]	91.53 [81.32, 97.19]	.6203 [.3196, .9211]
P2	14	3	41	1	82.35 [56.57, 96.20]	97.62 [87.43, 99.94]	93.33 [68.05, 99.83]	93.18 [81.34, 98.57]	93.22 [83.54, 98.12]	.8287 [.6677, .9898]
P3	8	2	45	4	80.00 [44.39, 97.48]	91.84 [80.40, 97.73]	66.67 [34.89, 90.08]	95.74 [85.46, 99.48]	89.83 [79.17, 0.96.18]	.6654 [.4189, .9120]
P4	3	1	53	2	75.00 [19.41, 99.37]	96.36 [87.47, 99.56]	60.00 [14.66, 94.73]	98.15 [90.11, 99.95]	94.92 [85.85, 98.94]	.6395 [.2629, 1.0000]
P6	3	1	55	0	75.00 [19.41, 99.37]	100.00 [93.51, 100.00]	100.00 [29.24, 100.00]	98.21 [90.45, 99.95]	98.31 [90.91, 99.96]	.8483 [.5570, 1.0000]
P1	7	5	45	2	58.33 [27.67, 84.83]	95.74 [85.46, 99.48]	77.78 [39.99, 97.19]	90.00 [78.19, 96.67]	88.14 [77.07, 95.09]	.5963 [.3288, .8638]
P10	1	2	54	2	33.33 [0.84, 90.57]	96.43 [87.69, 99.56]	33.33 [0.84, 90.57]	96.43 [87.69, 99.56]	93.22 [83.54, 98.12]	0.2976 [0, .8007]

TP, true positive; FN, false negative; TN, true negative; FP, false positive; PPV, positive predictive value; NPV, negative predictive value; Acc, accuracy; Agr, agreement between readers 1 and 2; P, partition

Additional findings

Additional diagnoses were achieved using MRI in 24/59 patients (40.67%), who were all affected by BME to some extent. These additional findings revealed AVN in 13 patients (22.03%) with 11 unilateral and 2 bilateral AVN cases, and insufficiency or stress fractures in 11 patients (18.64%). The additional findings were correctly identified in 23/24 patients (95.83%) by R1 and R2, who both missed two cases of AVN (one unilateral and one side of bilateral AVN) with 92.30% (24/26) overall detection rate.

Inter-observer agreements

The inter-observer agreement between R1 and R2, with regard to patients' analysis, was substantial ($k = 0.7065$, 95% CI 0.5055, 0.9074) and for the identification of additional findings, inter-observer agreement was very good ($k = 1.000$). Regarding partitions' analysis, inter-observer agreement ranged from 1.0000 to 0.8287 for 6/12 partitions (Table 3).

Discussion

This study evaluated the capabilities of DECT with VNCa applications to assess BME around the hip joint in a cohort of non-traumatic patients. The overall accuracy values in our results were similar to those of previous studies [21, 22, 24], in particular that of Kellock et al, which focused on the diagnosis of non-displaced hip fractures, obtaining a sensitivity of 77% and 91% (17 and 20 of 22 patients) and a specificity of 92–99% (89, 92, and 95 of 96 patients) for three readers using the VNCa application [21]. In another study focusing on non-displaced hip fractures, the quantitative analysis of DECT images (–55.3 HU cut-off) yielded 100% sensitivity, 94% specificity, and 95.4% accuracy [22].

In a recently published paper, Son et al used rapid kVp-switching dual-energy CT with water–HAP to identify BME in 40 patients with non-traumatic hip pain. The authors assessed 25 hips suffering from osteonecrosis and 18 hips suffering from osteoarthritis [24]. The authors focused on the evaluation of femoral BME, reporting an AUC of 0.96 for reader 1 and 0.91 for reader 2 for diagnosing BME. The sensitivity and specificity were 85% and 85% for reader 1 and 93% and 73% for reader 2, respectively [24]. However, other regions, including the pubis, iliac bone, or sacroiliac joints, were not included in the analysis and only water–HAP images, without conventional CT images, were assessed, in order to reduce bias [24]. Also, dual-source VNCa images have recently been used to identify BME around the ankle joint in a subgroup of 16 non-traumatic patients [26]. In the said study, the overall sensitivity, specificity, and accuracy achieved by

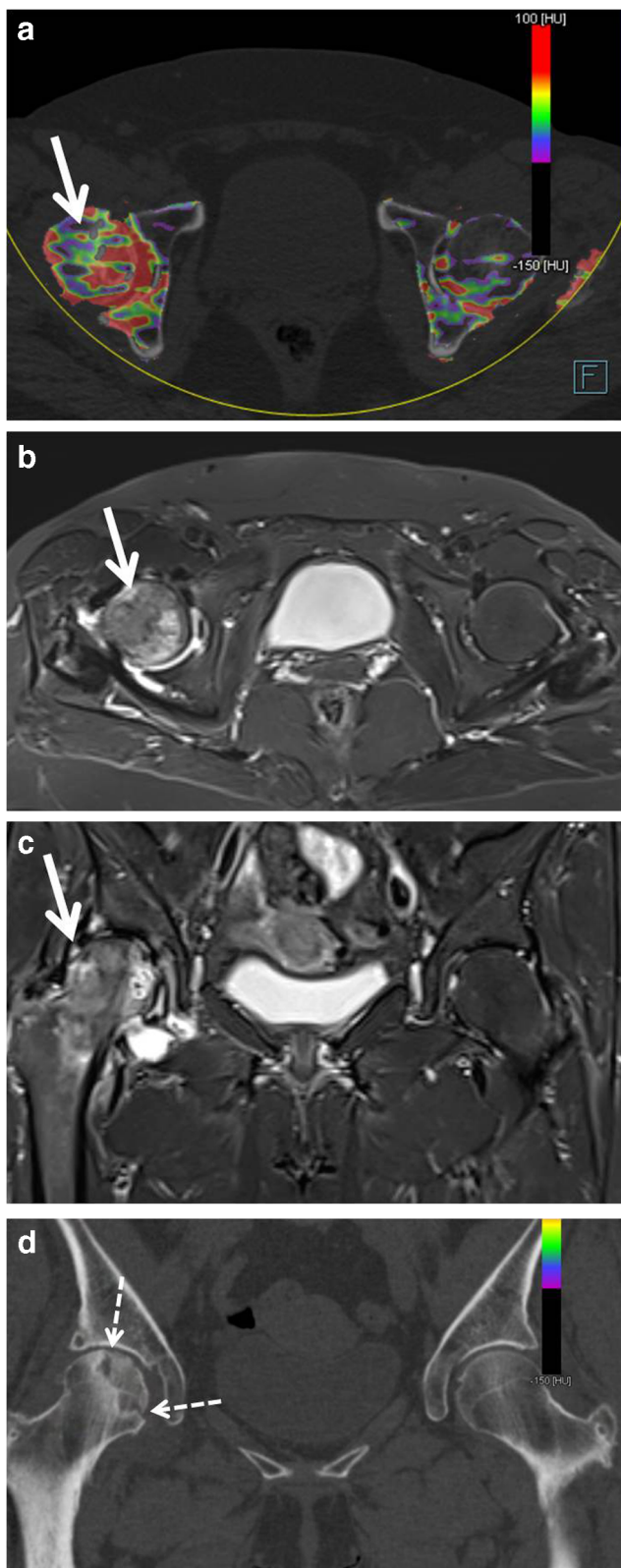


Fig. 2 Seventy-one-year-old woman with worsening hip pain due to advanced stage of AVN of the right femoral head. On the axial DECT 1-mm reconstructed image at the level of femoral heads (a), BME (arrow) can be depicted on the right side, with respect to the left femoral head. The superimposed DECT map was set to maximally enhance the presence of BME areas (coded between violet-blue and orange-red, representing mild and severe edema, respectively), and the spared areas coded as normal bone (because of densities under the expected cut-off). The presence of BME (arrow) is confirmed on the corresponding axial (b) and coronal T2 fat-saturated MRI (c) images. In the corresponding 1-mm coronal reconstructed DECT image (d), once removed, the superimposed BME map is possible to detect the presence of a large fracture line going from central to medial aspect of the femoral head (dotted arrows)

sensitivity and 80.00% specificity. The difference between the two readers could be explained by their different degrees of experience, particularly regarding their use of DECT, which were 6 years for R1 and 1 year for R2.

Further to this, the accuracy of both readers was influenced by the entity of signal alteration on the corresponding MRI images. As concerns the patients' analysis, the BME detection rates of R1 and R2 were 91.30% and 73.91% in the subgroup of patients suffering from mild edema. Conversely, all 21 patients, scored with severe BME at MRI, were correctly diagnosed by DECT. However, given that density values can vary drastically around the hip, we did not perform a quantitative analysis of DECT numbers.

Similarly, in a study by Cao et al [27], when grade 3–4 bone marrow was regarded as a positive result, VNCa images had relatively high predictive values for detection of bone marrow lesions (BML).

Bone sclerosis can represent an important pitfall in DECT imaging of the hip, as has been previously described for other anatomic sites [26–28]. Sclerosis is typically identified on the femoral head and acetabular roof, especially in elderly patients suffering from degenerative osteoarthritis of the hip, and at sites near to the pubis and sacroiliac joints. The changes in CT density associated with sclerosis can therefore result in DECT false positive findings, mimicking an area of BME. This is particularly true for pubis and sacroiliac joints. In such cases, an evaluation of standard CT images may show bilateral bone sclerosis and exclude associated findings (namely erosions or insufficiency fractures) so helping to avoid misdiagnosis. Conversely, markedly sclerotic bone can generate an artifact (due to excessive subtraction processes) that can hinder BME detection. Moreover, the possible drop in the accuracy of DECT in cases of subtle changes identified by MRI has been previously described [27]. Structural bone changes including subchondral cysts and bone sclerosis could be misinterpreted as edema in water–HAP imaging, as well [24]. The inter-observer agreement regarding the identification of additional findings ($k = 1.000$) and that regarding the identification of BME on the right ($k = 0.8287$) and left ($k = 0.8381$) femoral heads were most impressive. Indeed, the additional findings of our study were all associated with some

evaluating the DECT images were 92.0, 86.6, and 90.0% for reader 1 and 88.0, 86.6, and 87.5% for reader 2 [26].

As concerning patients' analysis, R1 achieved 95.45% sensitivity and 86.67% specificity, whereas R2 achieved 86.36%

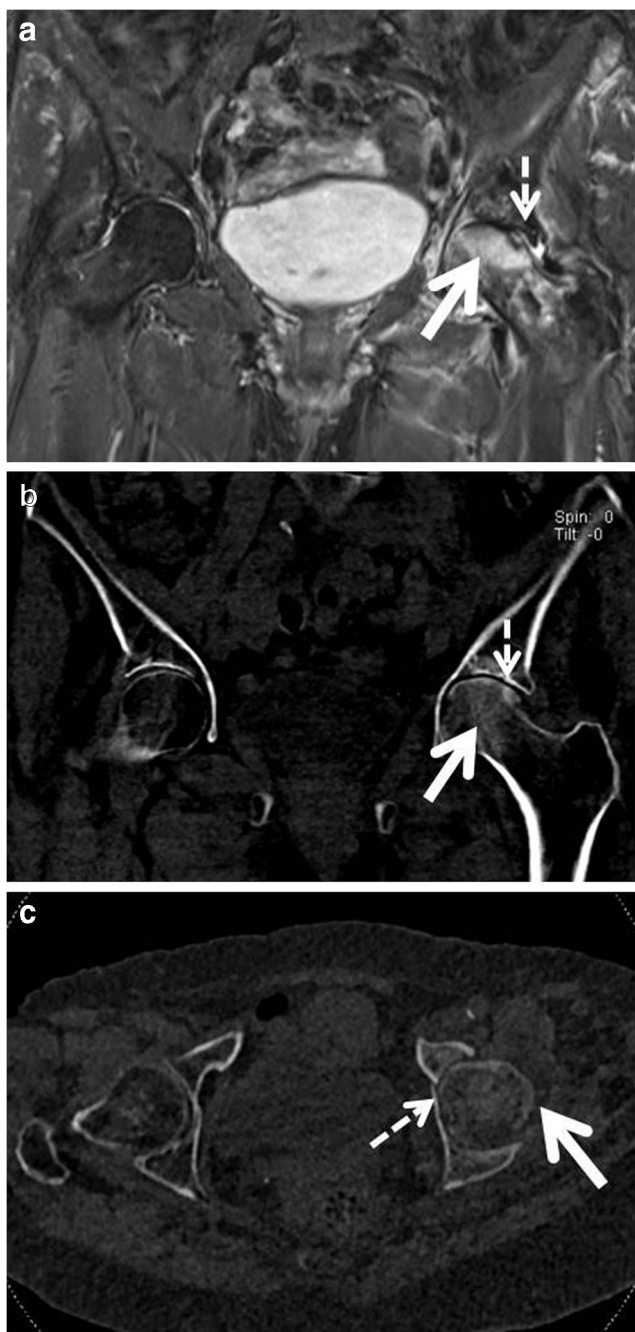


Fig. 3 Sixty-six-year-old woman with worsening left hip pain. On the coronal T2 fat-saturated MRI (a), BME can be recognized on the left acetabular roof and femoral head with relative sparing of medial aspect (arrow). A subchondral linear hypointense line is depicted (dotted arrow). On the corresponding reconstructed 1-mm coronal DECT image (b), the BME is characterized by an increased density (arrow) with respect to the right femoral head. A subchondral linear hyperdense line is depicted (dotted arrow), considered as a healing fracture. On the axial 1-mm reconstructed DECT image (c), BME can be confirmed by an increased density of the left femoral head and acetabulum (arrow). A tiny fracture of the acetabulum can be recognized (dotted arrow)

BME around the hip. Consequently, BME may help radiologists to identify and focus on subtle imaging findings. For example, BME may indicate early AVN. Also, BME may

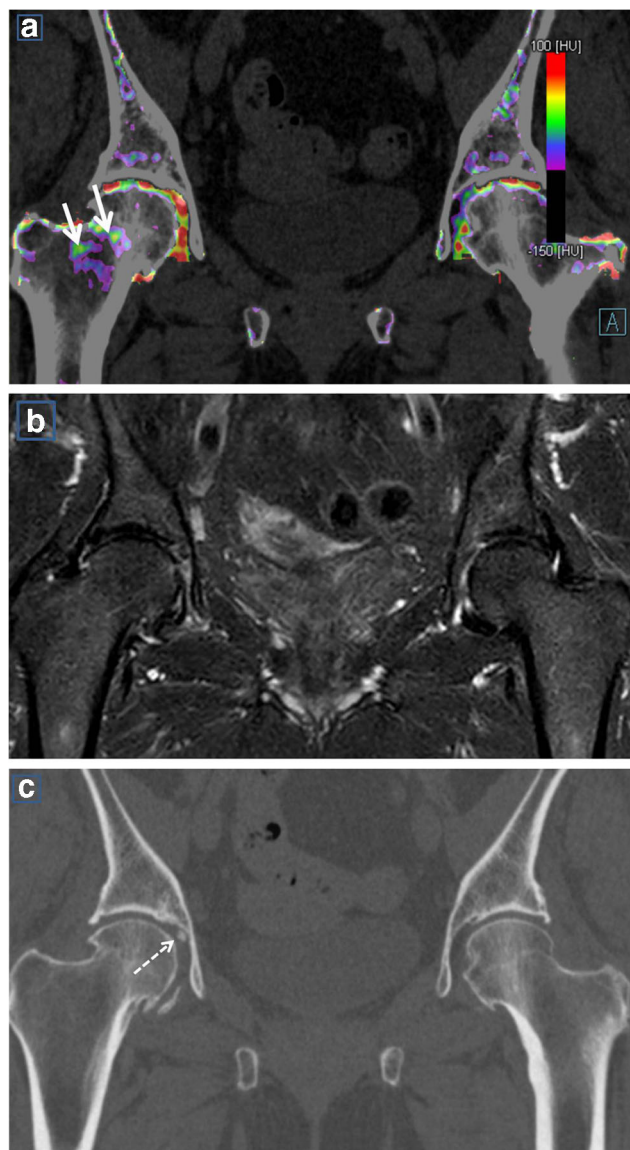


Fig. 4 Fifty-one-year-old man with right non-traumatic hip pain. On the coronal 1-mm reconstructed DECT image (a), some mild BME, coded as a superimposed violet to green area, is pointed out at the level of the right femoral neck (arrows). This represented a FP finding since the corresponding coronal T2 fat-saturated MRI ruled out the presence of BME (b). On the corresponding coronal 1-mm reconstructed CT image (c), an articular calcification is depicted on the right side, as a possible cause of groin pain (dotted arrow). The FP area of the right femoral neck does not correspond to areas of increased density

indicate an advanced stage of AVN, when it is associated with signs of collapse [29–31]. DECT could play a key role in the clinical management of patients with suspected AVN, confirming the presence of BME (pre-collapsed stages) and finely evaluating all anatomical changes relating to any collapse of the femoral head.

In our study, the additional findings were correctly identified by reading DECT images in 24/26 cases (96.15%) by both readers. However, both readers missed two cases of AVN because of sclerosis covering the underlying bone and

consequently altering the DECT numbers. It is important to note that both patients reported pain relief after having recently undertaken therapy, and that their BME was scored as mild using MRI.

The presence of stress or insufficiency fractures was diagnosed by MRI in 11 patients. All the fractures were correctly imaged at DECT, and BME was correctly indicated in all of these patients. The accuracy of DECT did not change with the varying location of the fractures, including the femoral neck, femoral head, iliac bone, and sacrum.

As previously suggested [24], in cases of groin pain presenting with BME as determined by DECT, the diagnosis of AVN or an insufficiency or stress fracture could be achieved with the concurrent reading of standard high-resolution CT images. Also, the presence of associated imaging finding may help radiologists in detecting BME. The presence of BME on partition 2 (right femoral head) was identified with 82.35% sensitivity, 97.62% specificity, and 93.22% accuracy, whereas the presence of BME on partition 8 (left femoral head) was identified with 83.33% sensitivity, 97.87% specificity, and 94.92% accuracy. We also achieved high values of agreement between readers regarding the evaluation of femoral head partitions (partition 2, $k = 0.8287$; partition 8, $k = 0.8381$).

This study has its limitations. Firstly, only a qualitative analysis of BME was performed in this paper. Studying multiple anatomic regions with different density values, several cut-off values would be required to perform a quantitative analysis of DECT numbers. However, the main scope of this study was to evaluate the overall accuracy of DECT in the evaluation of BME. Even if a subanalysis of single partition was performed, the number of positive findings in some of these partitions would not be sufficient to generate a reliable cut-off. Moreover, due to the lack of pathological correlation, AVN was not graded, and a dedicated analysis of AVN and fractures was not carried out in this study. Our data set did include patients suffering from advanced AVN (mainly women aged over 60 years) but there were few cases diagnosed as early-stage AVN, perhaps as our study population included relatively few young men, a category of patients that is typically diagnosed with early-stage AVN. Furthermore, we did not have available detailed clinical data for the patients enrolled regarding the cause of development of AVN or stress fractures, including use of medication and/or the presence of osteoporosis. Further studies in the future may help to understand if DECT could be reliable for accurately grading AVN and to demonstrate its role in patients at risk for the development of AVN.

In conclusion, our results confirmed that DECT has high overall diagnostic accuracy in depicting BME around the hip joint when compared to MRI, among a cohort of non-traumatic patients suffering from hip pain. Furthermore, DECT maps may help in the identification of additional

imaging findings often associated with BME, including AVN of the femoral head and insufficiency or stress fractures.

Acknowledgments Elinor Julie Rae Anderson for English editing.

Funding information The authors state that this work has not received any funding.

Compliance with ethical standards

Guarantor The scientific guarantor of this publication is Giovanni Foti.

Conflict of interest The authors of this manuscript declare no relationships with any companies, whose products or services may be related to the subject matter of the article.

Statistics and biometry Ronaldo Silva, PhD, kindly provided statistical advice for this manuscript.

Informed consent Written informed consent was obtained from all subjects (patients) in this study.

Ethical approval Institutional Review Board approval was obtained.

Methodology

- Prospective
- Diagnostic or prognostic study
- Performed at one institution

References

1. Vassalou EE, Spanakis K, Tsifountoudis IP, Karantanis AH (2019) MR imaging of the hip: an update on bone marrow edema. *Semin Musculoskelet Radiol* 23:276–288
2. Eustace S, Keogh C, Blake M, Ward RJ, Oder PD, Dimasi M (2001) MR imaging of bone oedema: mechanisms and interpretation. *Clin Radiol* 56:4–12
3. Murphey MD, Foreman KL, Klassen-Fischer MK, Fox MG, Chung EM, Kransdorf MJ (2014) From the radiologic pathology archives imaging of osteonecrosis: radiologic-pathologic correlation. *Radiographics* 34:1003–1028
4. Klontzas ME, Vassalou EE, Zibis AH, Bintoudi AS, Karantanis AH (2015) MR imaging of transient osteoporosis of the hip: an update on 155 hip joints. *Eur J Radiol* 84:431–436
5. Plakseychuk AY, Shah M, Varitimidis SE, Rubash HE, Sotereanos D (2001) Classification of osteonecrosis of the femoral head: reliability, reproducibility, and prognostic value. *Clin Orthop Relat Res* 386:34–41
6. Sen RK, Tripathy SK, Aggarwal S, Marwaha N, Sharma RR, Khandelwal N (2012) Early results of core decompression and autologous bone marrow mononuclear cells instillation in femoral head osteonecrosis: a randomized control study. *J Arthroplasty* 27:679–686
7. Agarwala S, Shah SB (2011) Ten-year follow-up of avascular necrosis of femoral head treated with alendronate for 3 years. *J Arthroplasty* 26:1128–1134
8. Marker DR, Seyler TM, Ulrich SD, Srivastava S, Mont MA (2008) Do modern techniques improve core decompression outcomes for hip osteonecrosis? *Clin Orthop Relat Res* 466:1093–1103

9. Yoo MC, Kim KI, Hahn CS, Parvizi J (2008) Long-term followup of vascularized fibular grafting for femoral head necrosis. *Clin Orthop Relat Res* 466:1133–1140
10. Ficat RP (1985) Idiopathic bone necrosis of the femoral head. Early diagnosis and treatment. *J Bone Joint Surg Br* 67:3–9
11. Zibis AH, Karantanas AH, Roidis NT et al (2007) The role of MR imaging in staging femoral head osteonecrosis. *Eur J Radiol* 63:3–9
12. Sakai T, Sugano N, Nishii T, Haraguchi K, Ochi T, Ohzono K (2000) MR findings of necrotic lesions and the extralesional area of osteonecrosis of the femoral head. *Skeletal Radiol* 29:33–141
13. Kim YM, Oh HC, Kim HJ et al (2000) The pattern of bone marrow oedema on MRI in osteonecrosis of the femoral head. *J Bone Joint Surg Br* 82:837–841
14. Stevens K, Tao C, Salem N et al (2003) Subchondral fractures in osteonecrosis of the femoral head: comparison of radiography, CT, and MR imaging. *AJR Am J Roentgenol* 180:363–368
15. Meier R, Kraus TM, Schaeffeler C et al (2014) Bone marrow oedema on MR imaging indicates ARCO stage 3 disease in patients with AVN of the femoral head. *Eur Radiol* 24:2271–2278
16. Mitchell DG, Rao V, Dalinka M et al (1986) MRI of joint fluid in the normal and ischemic hip. *AJR Am J Roentgenol* 146:1215–1218
17. Kubo T, Yamazoe S, Sugano N et al (1997) Initial MRI findings of non-traumatic osteonecrosis of the femoral head in renal allograft recipients. *Magn Reson Imaging* 15:1017–1023
18. Ikemura S, Yamamoto T, Motomura G, Nakashima Y, Mawatari T, Iwamoto Y (2010) MRI evaluation of collapsed femoral heads in patients 60 years old or older: differentiation of subchondral insufficiency fracture from osteonecrosis of the femoral head. *AJR Am J Roentgenol* 195:63–68
19. Narváez JA, Narváez J, De Lama E, De Albert M (2010) MR imaging of early rheumatoid arthritis. *Radiographics* 30:143–163
20. Barille MF, Wu JS, McMahon CJ (2014) Femoral head avascular necrosis: a frequently missed incidental finding on multidetector CT. *Clin Radiol* 69:280–285
21. Kellock TT, Nicolaou S, Kim SS et al (2017) Detection of bone marrow edema in nondisplaced hip fractures: utility of a virtual noncalcium dual-energy CT application. *Radiology* 284:798–805
22. Jang SW, Chung BM, Kim WT, Gil JR (2019) Nondisplaced fractures on hip CT: added value of dual-energy CT virtual non-calcium imaging for detection of bone marrow edema using visual and quantitative analyses. *Acta Radiol* 60:1465–1473. <https://doi.org/10.1177/0284185119831690>
23. Baffour FI, Glazebrook KN, Morris JM et al (2019) Clinical utility of virtual noncalcium dual-energy CT in imaging of the pelvis and hip. *Skeletal Radiol* 48:1833–1842
24. Son W, Park C, Jeong HS, Song YS, Lee IS (2019) Bone marrow edema in non-traumatic hip: high accuracy of dual-energy CT with water-hydroxyapatite decomposition imaging. *Eur Radiol*. <https://doi.org/10.1007/s00330-019-06519-8>
25. Laukamp KR, Lennartz S, Neuhaus VF et al (2018) CT metal artifacts in patients with total hip replacements: for artifact reduction monoenergetic reconstructions and post-processing algorithms are both efficient but not similar. *Eur Radiol* 28:4524–4533
26. Foti G, Catania M, Caia S et al (2019) Identification of bone marrow edema of the ankle: diagnostic accuracy of dual-energy CT in comparison with MRI. *Radiol Med* 124:1028–1036
27. Cao JX, Wang YM, Kong XQ, Yang C, Wang P (2015) Good interrater reliability of a new grading system in detecting traumatic bone marrow lesions in the knee by dual energy CT virtual noncalcium images. *Eur J Radiol* 84:1109–1115
28. Wang CK, Tsai JM, Chuang MT, Wang MT, Huang KY, Lin RM (2013) Bone marrow edema in vertebral compression fractures: detection with dual-energy CT. *Radiology* 269:525–533
29. Yamamoto S, Watanabe A, Nakamura J et al (2011) Quantitative T2 mapping of femoral head cartilage in systemic lupus erythematosus patients with noncollapsed osteonecrosis of the femoral head associated with corticosteroid therapy. *J Magn Reson Imaging* 34:1151–1158
30. Hofmann S, Schneider W, Breitenseher M, Urban M, Plenk H Jr (2000) “Transient osteoporosis” as a special reversible form of femur head necrosis. *Orthopade* 29:411–419
31. Iida S, Harada Y, Shimizu K et al (2000) Correlation between bone marrow edema and collapse of the femoral head in steroid-induced osteonecrosis. *AJR Am J Roentgenol* 174:735–743

Publisher's note Springer Nature remains neutral with regard to jurisdictional claims in published maps and institutional affiliations.